Monthly Notices of the ROYAL ASTRONOMICAL SOCIETY
MNRAS **507,** 3698–3706 (2021) https://doi.org/10.1093/mnras/stab2404

Signature of the turbulent component of the solar dynamo on active region scales and its association with flaring activity

Valentina I. Abramenko*
Crimean Astrophysical Observatory, Russian Academy of Science, Nauchny, Bakhchisaray, 298409, Crimea, Russia

Accepted 2021 August 17. Received 2021 August 14; in original form 2021 April 6

ABSTRACT

It is a challenging problem to obtain observational evidence of the turbulent component of solar dynamo operating in the convective zone because the dynamo action is hidden below the photosphere. Here we present results of a statistical study of flaring active regions (ARs) that produced strong solar flares of an X-ray class X1.0 and higher during a time period that covered solar cycles 23 and 24. We introduced a magneto-morphological classification of ARs, which allowed us to estimate the possible contribution of the turbulent component of the dynamo into the structure of an AR. We found that in 72 per cent of cases, flaring ARs do not comply with the empirical laws of the global dynamo (frequently they are not bipolar ARs or, if they are, they violate the Hale polarity law, the Joy law, or the leading sunspot prevalence rule). This can be attributed to the influence of the turbulent dynamo action inside the convective zone on spatial scales of typical ARs. Thus, it appears that the flaring is governed by the turbulent component of the solar dynamo. The contribution into the flaring from these AR 'violators' (irregular ARs) is enhanced during the second maximum and the descending phase of a solar cycle, when the toroidal field weakens and the influence of the turbulent component becomes more pronounced. These observational findings are in consensus with a concept of the essential role of non-linearities and turbulent intermittence in the magnetic fields generation inside the convective zone, which follows from dynamo simulations.

Key words: diffusion – turbulence – Sun: magnetic fields – Sun: photosphere.

1 INTRODUCTION

With improved astrophysical observational and computational capabilities, new evidence has been presented that magnetic fields are the key force that supports the endless chain of cosmological non-stationary phenomena. In space, a magnetic field generates energy from stars and galaxies. This small amount of energy under the influence of the weak seed magnetic field and turbulent motions in the medium is spent on the generation of new magnetic flux, the so-called dynamo process. Release of this magnetic energy fuels the relentless activity of solar-type stars, including spots and eruptions (flares on the Sun).

Studies of the solar dynamo and investigations in the field of solar flare forecasting usually do not overlap. Theoretical research and numerical simulations of the dynamo do not consider the problems of solar flares; see, for example, Karak & Miesch (2017), Pipin (2018) and Cameron et al. (2018), and see also reviews by Charbonneau (2010, 2014, 2020) and Brun et al. (2015). In turn, recent progress in flare forecasting (e.g. Barnes et al. 2016; Leka et al. 2019; Cinto et al. 2020; Nishizuka et al. 2020) is often based on the photospheric magnetic field properties of active regions (ARs) with statistical and machine learning techniques and does not involve processes of magnetic flux generation. Here we explore solar activity by studying dynamo processes and we show that the non-linear (turbulent) component of the dynamo (i.e. fluctuations of the dynamo on a broad range of spatial scales) is connected to variations of flaring activity. These fluctuations can be revealed from observations. It is widely accepted that, for the majority of solar ARs, the magnetic field is generated by the mean-field dynamo (global dynamo); see, for example, a review by van Driel-Gesztelyi & Green (2015). According to Abramenko, Zhukova & Kutsenko (2018), the magnetic structure of about 70 per cent of the investigated 1494 ARs is consistent with the essential empirical laws that follow from the mean-field dynamo theory: bipolar ARs obeying the Hale polarity law, the Joy law and the rule of a prevalence of the leading spot in a bipolar structure. Nevertheless, the question of how to explain the appearance of those 30 per cent of ARs that violate the aforementioned laws is still open. It is highly unlikely that these ARs are simply a result of large fluctuations in a Gaussian medium because a fraction of such fluctuations should not exceed 5 per cent. One possibility is to consider them to be the result of strong fluctuations in an intermittent medium; in other words, in a non-linear dynamical dissipative system (NLDDS). In such a system, strong fluctuations are not rare and they appear in both space and time domains. In this case, there is a basis to speculate that strong flares are intrinsically related to strong spatial fluctuations (i.e. ARs that violate the mean-field theory rules mentioned above). It is well established that ARs with a complex magnetic structure display enhanced flare activity (e.g. Ireland et al. 2008; Falconer, Moore & Gary 2008; McAteer, Gallagher & Conlon 2010). However, there are also alternative opinions on this subject (e.g. Georgoulis 2012). The majority of publications are focused on revealing the critical conditions for flares to occur, and on finding a set of parameters that are sensitive to the build up of pre-flare energy. Our approach is different. We consider strong flares as unavoidable strong fluctuations in the time domain.

* E-mail: vabramenko@gmail.com

For an NLDDS, the presence of strong temporal fluctuations also implies the existence of strong deviations in the spatial domain. In our case, strong spatial fluctuations are the AR 'violators' (irregular ARs) with deviations from the regular magnetic configuration. If the solar dynamo performs as a NLDDS, then the occurrence of strong flares and the appearance of AR violators have to be statistically related. We intend to check this hypothesis. To do this, we have investigated all 79 ARs of solar cycles 23 and 24 that produced at least one X-class flare during its passage across the solar disc. For each AR, we determined its magneto-morphological classification (MMC) by using the criteria outlined below, and we compared these with the flaring index of the AR. A time distribution of the ARs through the cycles was also analysed to reveal the signature of the dynamo wave performance.

2 MAGNETO-MORPHOLOGICAL CLASSIFICATION OF ACTIVE REGIONS

According to the mean-field dynamo theory, the flux tubes of the toroidal field rise from the bottom of the convection zone toward the photosphere and then form bipolar magnetic regions (sunspot groups, or ARs) as that flux pushes further into the solar atmosphere. For the majority of cases, the sunspot groups obey certain empirical laws (van Driel-Gesztelyi & Green 2015). Thus, polarities of the leading (western) sunspot are opposite in the Northern and Southern hemispheres, and the polarity sign changes from one cycle to another cycle, a behaviour known as the Hale polarity law (Hale et al. 1919; Hale & Nicholson 1925). Bipolar ARs tend to emerge with a systematic tilt of their axis relative to the solar equator, so that the leading sunspot is located closer to the equator. The tilt tends to increase with the latitude and this pattern is known as the Joy law. The twist of an emerging flux tube is determined by the Coriolis force and is thought to be a plausible reason for the tilt (Wang & Sheeley 1991; D'Silva & Choudhuri 1993); however, there are other possible reasons (Leighton 1969; McClintock & Norton 2013). The third empirical law is the prevalence of the leading sunspot in the bipolar structure; in the majority of cases, the area of the leading spot is larger than the area of the largest sunspot in the following part of an AR. This implies that the leading spot is more coherent and the magnetic fields are less inclined than those in the following part. Note that Babcock (1961) considered this observational property of bipolar ARs as one of the keystones of the Babcock–Leighton phenomenological concept of the solar dynamo, which later became the origin of the mean-field dynamo theory.

However, as mentioned in the Introduction, about one-third of ARs do not follow these laws (Abramenko et al. 2018). The tilt of a bipolar structure might not follow the Joy law (the most common violation, in 20 per cent of all ARs), the leading spot might be smaller than the largest following spot (about 12 per cent of the total number) or the polarities of leading and following spots might be reversed (anti-Hale ARs, which constitute about 3–4 per cent of all ARs). All these deviations can be explained by peculiarities in the flow field of the convection zone that twist and stretch a toroidal flux rope while it rises toward the photosphere; in other words, by the mild influence of the turbulent dynamo.

The influence of the turbulent dynamo on the toroidal flux ropes can be stronger. For example, it can result in fragmentation of a flux rope with subsequent deformation of the fragments that can lead to the formation of several coaligned bipoles on the solar surface with prevailing east–west orientation, similar to the well-known AR, NOAA 11158. Moreover, distortions of the toroidal flux rope can become so significant that the resulting AR may appear as a complex configuration of mixed polarity sunspots distributed chaotically.

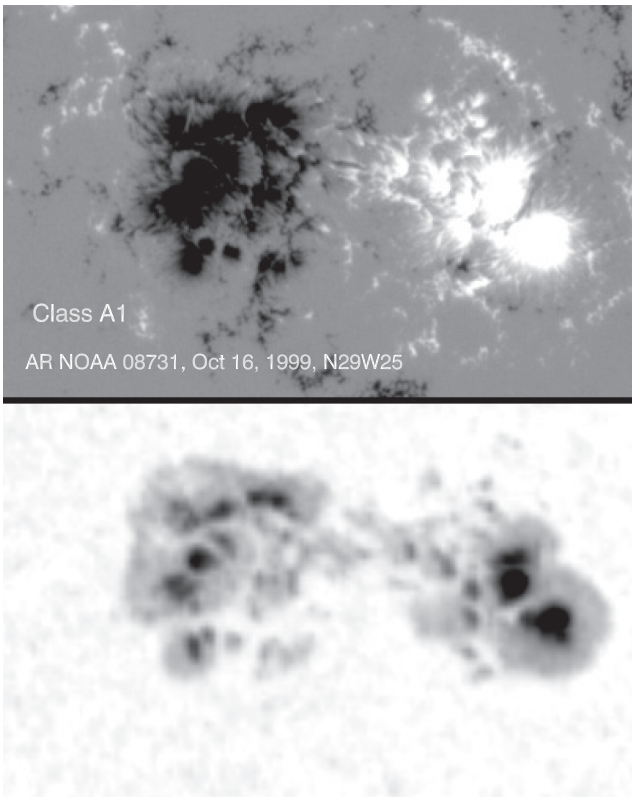

Figure 1. A typical example of an AR of the A1 class: a bipolar AR of solar cycle 23 is located in the Northern hemisphere and has the positive polarity of the leading spot (compliance of the Hale polarity law). The AR obeys the Joy law and the leading spot dominates any of the following spots. No small δ-structure is observed. The magnetogram (top) and the continuum image (bottom) are acquired in high-resolution mode by the Michelson Doppler Imager (MDI) on the *Solar and Heliospheric Observatory* (*SOHO*; Scherrer et al. 1995). North is to the top, and west to the right. The direction of the equator coincides with the horizontal side of the frame. The magnetogram is scaled from −800 G (black) to 800 G (white).

In our original MMC (Abramenko et al. 2018), we divided all ARs into three classes: class A, which includes bipolar ARs that follow all aforementioned laws, refers to regular ARs; class U consists of unipolar sunspots without opposite polarity pores in the trailing part, and class B includes the rest of the ARs (i.e. irregular ARs). Some irregular ARs have a bipole structure and violate at least one of the laws. However, some of them do not display a classical bipole structure; instead, they show multipolar or strong δ-structures. The multipolar and strong δ-structures were very rare when we studied ARs of any flaring capability, but they are not rare at all when we explore the strong-flaring ARs here. Strictly speaking, the three aforementioned laws are not applicable for ARs without a classical bipolar structure. This motivated us to introduce here further specifications inside the classes.

Considering that the aim of this study is to estimate the degree of influence of the turbulent dynamo on the AR formation process, we have modified our classification (Abramenko et al. 2018) by introducing subclasses into the A and B classes, as follows.

A1: bipolar ARs for which the Hale polarity law and the Joy law are fulfilled, the leading spot is dominant, and there are no small δ-structures inside the AR during its passage across the solar disc

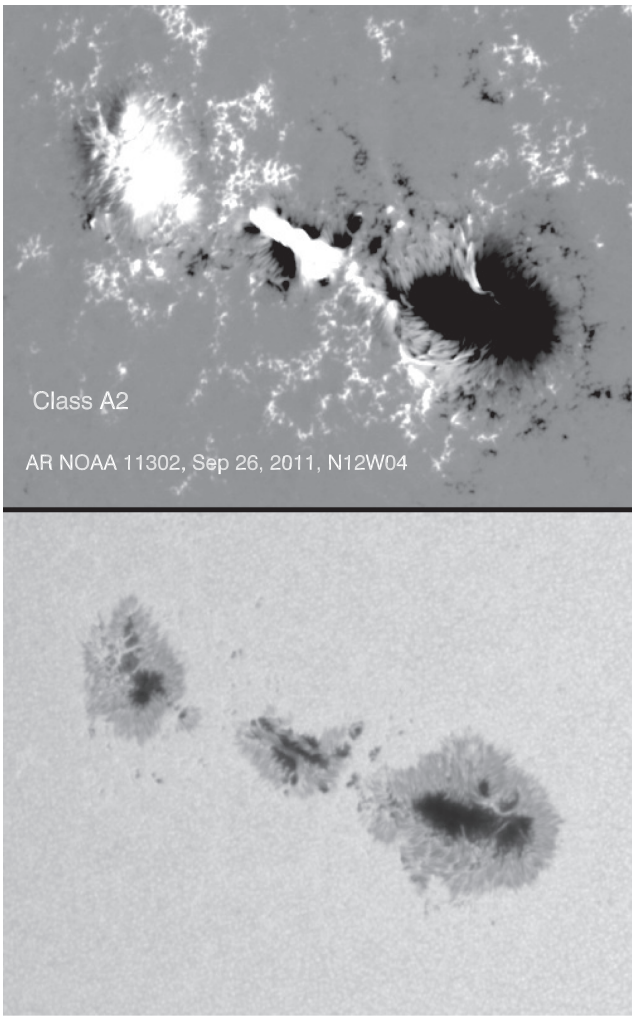

Figure 2. A typical example of an AR of the A2 class: a bipolar AR of solar cycle 24 is located in the Northern hemisphere and has the negative polarity of the leading spot (compliance of the Hale polarity law). The AR obeys the Joy law and the leading spot dominates the following spot. A small δ-structure is observed in the middle. The line-of-sight magnetogram (hmi.sharp-720s series) and the continuum image are acquired by the Helioseismic and Magnetic Imager (HMI) onboard the *Solar Dynamic Observatory (SDO*; Schou et al. 2012). North is to the top, and west to the right. The direction of the equator coincides with the horizontal side of the frame. The magnetogram is scaled from −500 G (black) to 500 G (white).

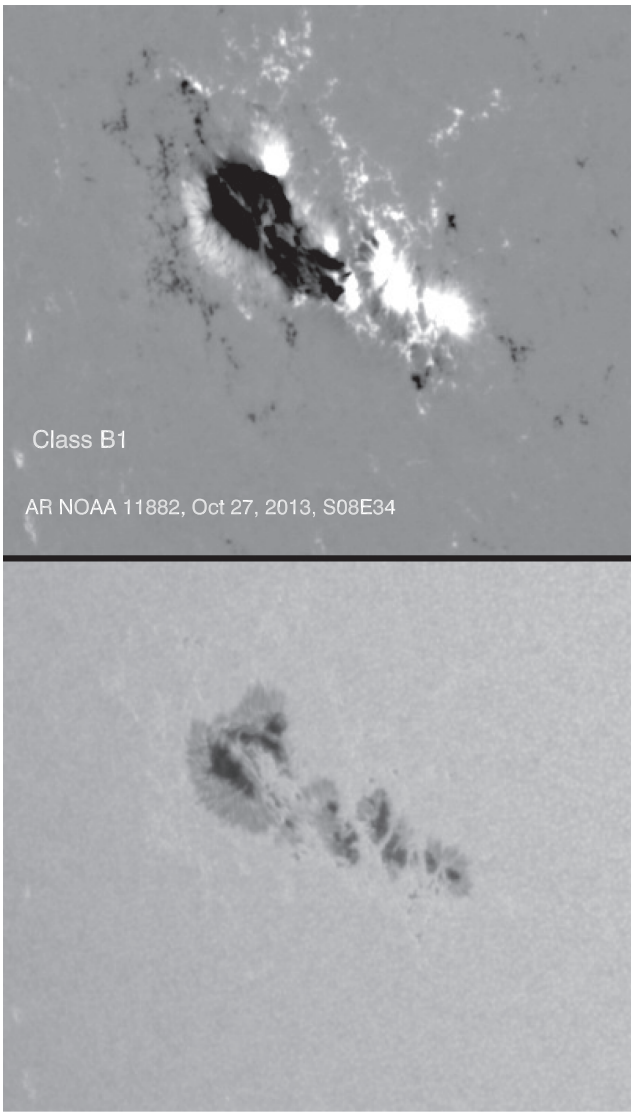

Figure 3. A typical example of an AR of the B1 class: a bipolar AR of solar cycle 24 is located in the Southern hemisphere and has the positive polarity of the leading spot (compliance of the Hale polarity law). The AR does not obey the Joy law, the leading part is located farther from the equator than the following part, the rule of the prevalence of the leading spot is not met, and the leading spot is smaller than the following spot. Notations are the same as in Fig. 2.

(see Fig. 1). These types of ARs can be considered to be the result of the non-disturbed emergence of a single toroidal flux tube.

A2: bipolar ARs for which the Hale polarity law and the Joy law are fulfilled, the leading spot dominates, and there are small (relative to the size of the leading spot) δ-structure(s) during the passage across the solar disc (see Fig. 2). These types of ARs may result from a small contribution of the turbulent dynamo, possibly operating at the near-surface depth.

B1: bipolar ARs that violate at least one of the aforementioned laws (can be considered to be the result of mild distortion of a single toroidal flux tube), with small (if any) δ-structure(s) during the passage across the solar disc. A typical example is shown in Fig. 3.

B2: multipolar ARs consisting of several quasi-coaligned bipoles having a general axis orientation in accordance with the Joy law. Frequently, these ARs contain a strong δ-structure and they can be represented by the AR, NOAA 11158 (see Fig. 4). Class B2 ARs can be regarded as the result of fragmentation and distortion of a single toroidal flux tube. For this reason, we include in the B2 class strong single δ-structures (see fig. 15a in Toriumi & Wang 2019) also consisting of one flux tube.

B3: multipolar ARs where opposite polarity sunspots are distributed in an irregular manner so that it is impossible to define the AR axis and assign leading and trailing sunspots (see Fig. 5). These ARs represent the most complex magnetic structures and can be considered to be the result of interaction (intertwining) of several flux tubes in the convective zone. Often such magnetic knots appear in the vicinity of a unipolar sunspot (e.g. the AR, NOAA 12673) resulting from fast flux emergence. It is likely that such a bundle of interwound flux tubes may have been channelled to the surface along the pre-existing structures of deeply rooted stable sunspots.

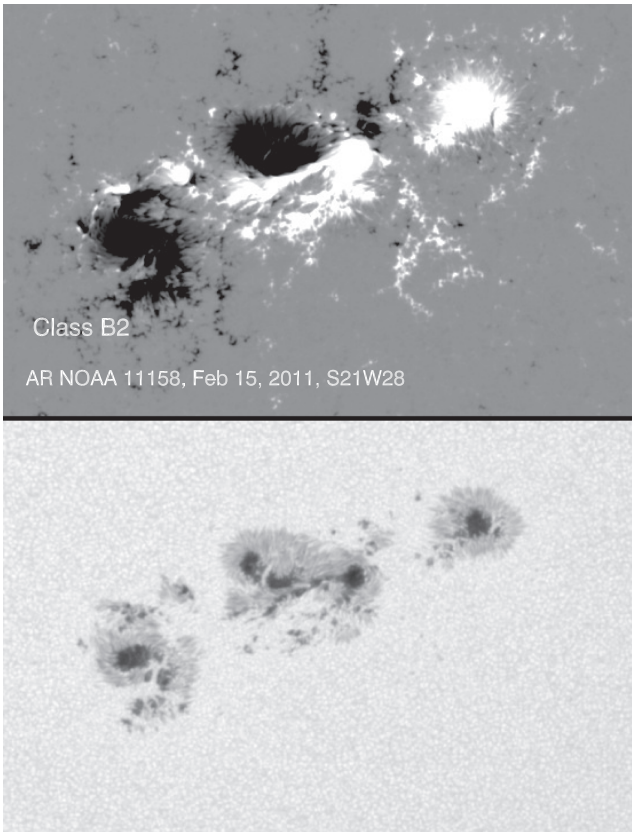

Figure 4. An example of an AR of the B2 class: a complex AR composed from two coaligned bipoles emerging simultaneously with the general orientation in accordance with the Joy law that allows us to suppose a common toroidal flux tube (fragmented or bended; see fig. 6 in Toriumi et al. 2017). The Hale polarity law and the Joy law are met for both bipoles, but the leading spot prevalence rule is not applicable. Notations are the same as in Fig. 2.

The existence of such a channel in the vicinity of a vortex structure – recall that $B = rot(A)$ – is a frequent occurrence in an intermittent medium (Frisch 1995).

Table 1 summarizes the essential criteria of the MMC. Our comments in the framework of turbulent dynamo influence are presented in parentheses.

We note that some ARs evolve very fast during their passage across the solar disc, so it is difficult to assign a permanent MMC class for the entire time interval. In such cases, we assign the class as determined during an interval of 2–3 d prior to the strongest flare. For ARs with the strongest flare occurring in the eastern limb, the class was acquired when the AR was on the longitude around −(50–70) degrees (e.g. the ARs, NOAA 12339 and 10930).

As for bipolar ARs, in the present study, we utilized an experience obtained in Abramenko et al. (2018) for reliable estimations of the AR's tilt (the Joy law) and the leading spot dominance. Problems that arise in detection of ARs with reverse polarity (violation of the Hale polarity law) are discussed in detail by Zhukova et al. (2020) and taken into account here. As for multipolar ARs, there could be some issues concerning which class (B2 or B3) a given AR should be assigned to. For example, in the AR, NOAA 12297, the dominating feature is the strong δ-structure, and the AR could be classified as B2. However, a moderate bipole nearby the δ-structure emerging during the day of the strongest flare makes it more favourable to classify this AR as B3 (i.e. a multipolar caused by at least two flux tubes).

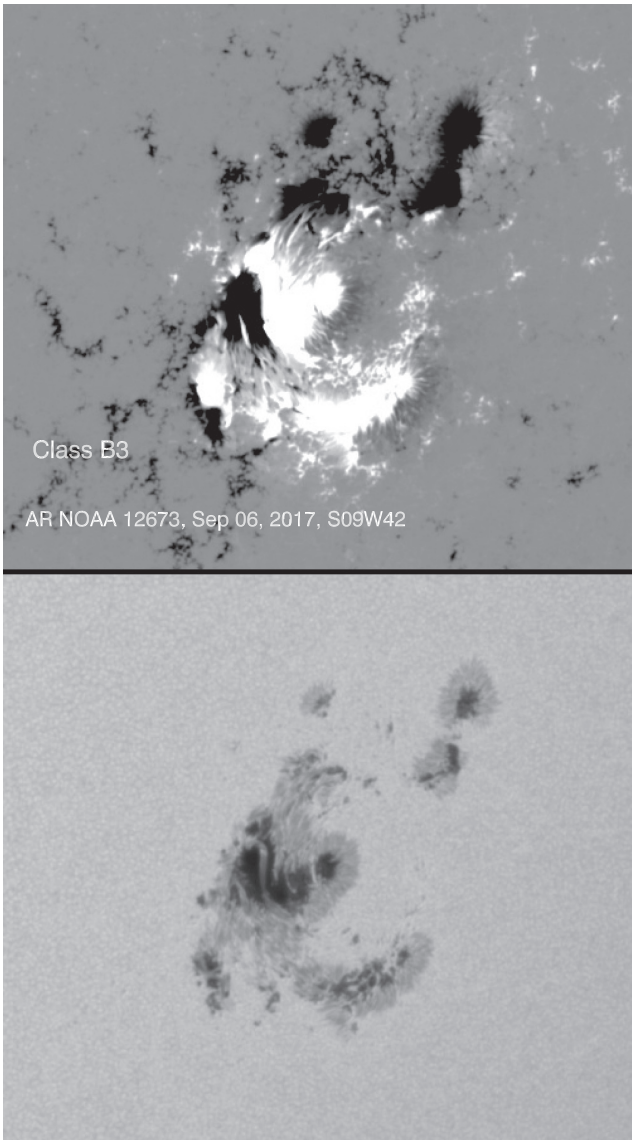

Figure 5. An example of an AR of the B3 class: a complex AR composed from several chaotically distributed spots of both polarities. The empirical global dynamo laws are not applicable. A complex knot of flux tubes in the convective zone, similar to that in fig. 4 of Ishii, Kurokawa & Takeuchi (1998), might be the source. Notations are the same as in Fig. 2.

Our list includes 79 ARs that produced X-class flares during the time interval from 1996 January to 2018 December spanning solar cycles 23 and 24 (see Tables 2 and 3). Only for nine ARs (out of 79) was no δ-structure observed and documented during all days of observations (see the last column in both tables). This allowed us to conclude that the presence of a δ-structure within an AR appears to be a common condition for an X-class flare to occur.

In this context, it is interesting to compare our classification with the classifications of δ-structures by Zirin & Liggett (1987) and by Toriumi & Wang (2019). Two opposite polarity umbras embedded in a common penumbra belong to type 1 according to Zirin & Liggett (1987) and comprise a 'spot–spot' type according to Toriumi & Wang (2019), while in our MMC classification this structure belongs to class B2. A multipolar complex of tightly packed sunspots within an extended penumbra ('island δ-spots') belongs to type 1 δ-structures according to Zirin & Liggett (1987) and to the B3 class in the

Table 1. MMC of all ARs except unipolar sunspots.

Panel A: regular ARs (bipolar ARs obeying the Hale polarity law, the Joy law and the leading spot prevalence rule)		Panel B: all the rest (irregular ARs)		
A1	A2	B1	B2	B3
Bipolar ARs obeying the Hale and Joy laws, and the leading spot prevalence rule, without any δ-structures. (Emergence of a single toroidal flux tube following the global dynamo rules.)	Bipolar ARs obeying the Hale and Joy laws, and the leading spot prevalence rule, with small δ-structure(s). (Emergence of a single toroidal flux tube following the global dynamo and minor influence of turbulent dynamo.)	Bipolar ARs violating at least one of the laws. (Emergence of a single toroidal flux tube rotated and/or inclined owing to the turbulent dynamo action.)	Multipolar ARs consisting of several coaligned bipoles (as a result of fragmentation and distortion of a single flux tube), or tight strong δ-structure. (As a result of strong twist of a single flux tube by the turbulent dynamo action.)	Multipolar ARs with chaotically distributed spots of both polarities. (Emergence of several interwound flux tubes by turbulent dynamo.)

MMC classification. ARs of type 2 (Zirin & Liggett 1987) and 'spot-satellite' ARs (Toriumi & Wang 2019), in cases when the satellite-sunspot is smaller than the leading spot, belong to the class of the hosting bipole. Type 3 ARs (Zirin & Liggett 1987) and 'quadrupole' groups (Toriumi & Wang 2019) overlap with class B2 in the MMC classification. 'Inter-AR' groups (Toriumi & Wang 2019) are very rare and belong to our B3 class (the AR, NOAA 08647; see table note *b* in Table 2).

We did not utilize the existing classifications such as the Zurich classification (or McIntosh Sunspot Group Classification; McIntosh 1990) and the Hale classification (Mount Wilson classification; Hale et al. 1919) for the following reasons. Both these classifications uniformly treat all bipolar ARs, which is not acceptable when the aim is to diagnose the turbulent dynamo in the convection zone. The advantages of the proposed classification are the following: (i) those bipoles violating the empirical laws of the global dynamo are separated into one special class; and (ii) the classification scheme is organized in such a way that the expected contribution from the turbulent dynamo increases through the classes from A1 to B3.

3 DISTRIBUTION OF STRONG-FLARING ACTIVE REGIONS OVER THE MMC

The second and third columns in Tables 2 and 3 list the first and last days of the AR's presence on the solar disc, while the fourth column lists the strongest X-class flare in an AR (GOES class, date and UT time). The fifth column shows the corresponding flare Index (FI; Abramenko 2005), which was derived by summing the GOES class of all flares observed in an AR during its passage across the solar disc, τ, and then normalizing the total by τ. Further scaling was applied so that an AR with one C1.0 (X1.0) flare per day has the flare index FI = 1.0 (100). The sixth column lists the AR compliance with the empirical laws of the global dynamo for the bipolar ARs. In the heading, the 'H' stands for the Hale polarity law, the 'J' stands for the Joy law and the 'L' for the dominance of the leading spot rule. In this column, 'Y' denotes 'Yes' (i.e. adhering to the law) and 'N' denotes 'No' (i.e. violation of the law). Multipolar ARs are marked with an 'M' and ARs with a strong dominating δ-structure are marked with 'δ'. The magneto-morphological class is shown in the next column. The final column shows the Hale class[1] of an AR determined prior to the flare. As mentioned above, the majority of ARs (70 out of 79) possess a δ-structure.

The MMC distribution of the analysed ARs is shown in Fig. 6. The majority of the X-class flare ARs (72 per cent) are of the B class. Also, the AR capability to produce intense flares tends to increase with the MMC, changing from A1 to B3; that is, with an enhanced complexity caused by the increasing contribution/influence of the turbulent component of the dynamo. (The only deviation is a transition from class A2 to B1 – the A2 ARs are more numerous than the B1 ARs. Apparently, the presence of even a small δ-structure is more important for strong flaring than the overall rotation or inclination of the flux tube.) In general, ARs of class A display low flare activity, with the most regular ones (A1 class) being the least active, and these are few in number. ARs with even a small δ-structure present (class A2) are more prone to strong flaring, and they are more numerous and display a higher flare index compared with the ARs in the A1 class. Similar dynamics can be seen for ARs within the B class; the strongest flares occur in ARs of classes B2 and B3 (i.e. those ARs that are most affected by the turbulent dynamo).

We would like to emphasize that ARs of the B class constitute about 25–30 per cent of all ARs, regardless of their flaring activity (Abramenko et al. 2018), whereas their fraction increases up to 72 per cent when we consider only those ARs with strong flares (>X1.0). This suggests that the occurrence of the most powerful flares is associated with those magnetic configurations for which the turbulent dynamo in the convective zone contributed substantially to the generation of their flux. Also, the larger the contribution of the turbulent dynamo action, the stronger the flaring potential of the resulting magnetic structure.

4 DISTRIBUTION OF STRONG-FLARING ACTIVE REGIONS ALONG A CYCLE

The cycle dependence in the appearance of flare-producing ARs is shown in Figs 7 and 8 where the AR flare index is plotted against the AR observation time. We also plot time variations of sunspot area using Royal Greenwich Observatory (RGO) and US Air Force (USAF) National Oceanic and Atmospheric Administration (NOAA) sunspot data[2] smoothed with a 13-month averaging window. Regular ARs in the A class are shown with black circles, and ARs in the B class are shown with red circles. ARs in the B class are more numerous and they appear throughout the entire cycle. ARs in the A class are mostly concentrated at the rising phase and the first maximum of each solar circle. There are no ARs in the A class with

[1]Hale classification data were taken from the following online sources: https://solarmonitor.org and http://solarcyclescience.com.

[2]http://solarcyclescience.com/activeregions.html

Table 2. ARs with X-class flares in solar cycle 23.

NOAA	Start	End	Max. flare (UT)	FI	H J L[a]	MMC class	Hale class
07978	1996.07.07	1996.07.13	X2.6 1996.07.09 (09:01)	46.85	M	B2	$\beta\gamma\delta$
08100	1997.10.27	2997.11.09	X9.4 1997.11.06 (11:49)	97.85	YYN	B1	$\beta\gamma\delta$
08113	1997.11.26	1997.12.09	X2.6 1997.11.27 (12:59)	36.00	YYY	A2	$\beta\gamma\delta$
08210	1998.04.25	1998.05.08	X1.1 1998.05.02 (13:31)	31.11	NYN	B1	$\beta\gamma\delta$
08307	1998.08.19	1998.09.02	X4.9 1998.08.18 (22:10)	72.74	YYN	B1	$\beta\delta$
08384	1998.11.09	1998.11.23	X2.2 1998.11.23 (06:28)	16.29	YYY	A2	$\beta\delta$
08647[b]	1999.07.25	1999.08.06	X1.4 1999.08.02 (21:18)	17.85	M	B3	$\beta\gamma$
08674	1999.08.20	1999.09.02	X1.1 1999.08.28 (17:52)	45.33	M	B3	$\beta\gamma\delta$
08731	1999.10.10	1999.10.23	X1.8 1999.10.14 (08:54)	18.52	YYY	A1	$\beta\gamma$
08771	1999.11.18	1999.11.29	X1.4 1999.11.27 (12:05)	36.81	YYY	A2	$\beta\gamma\delta$
08858	2000.02.03	2000.02.16	X1.2 2000.02.05 (19:17)	17.18	M	B3	β
08910	2000.03.12	2000.03.25	X1.8 2000.03.24 (07:41)	32.37	M	B3	$\beta\gamma\delta$
09026	2000.06.01	2000.06.14	X2.3 2000.06.06 (14:58)	70.07	δ	B2	$\beta\gamma\delta$
09033	2000.06.05	2000.06.19	X1.0 2000.06.18 (01:52)	15.04	YYY	A1	$\beta\gamma$
09077	2000.07.07	2000.07.21	X5.7 2000.07.14 (10:03)	92.96	M	B3	$\beta\gamma\delta$
09169	2000.09.18	2000.10.01	X1.2 2000.09.30 (23:13)	18.67	YYY	A1	$\beta\gamma\delta$
09236	2000.11.18	2000.12.01	X4.0 2000.11.26 (16:34)	98.22	YYY	A2	$\beta\gamma\delta$
09393	2001.03.23	2001.04.04	X20. 2001.04.02 (21:32)	218.59	M	B2	$\beta\gamma\delta$
09415	2001.04.03	2001.04.15	X14. 2001.04.15 (13:19)	208.20	δ	B2	$\beta\gamma\delta$
09511	2001.06.20	2001.06.30	X1.2 2001.06.23 (04:02)	24.17	YYY	A2	$\beta\gamma\delta$
09591	2001.08.22	2001.09.03	X5.6 2001.08.25 (16:23)	64.59	δ	B2	$\beta\gamma\delta$
09632	2001.09.20	2001.10.02	X2.6 2001.09.24 (09:32)	23.78	δ	B2	$\beta\gamma\delta$
09661	2001.10.11	2001.10.23	X1.6 2001.10.19 (00:47)	30.07	δ	B2	$\beta\gamma\delta$
09672	2001.10.18	2001.10.30	X1.3 2001.10.25 (14:42)	35.11	δ	B2	$\beta\gamma\delta$
09684	2001.10.28	2001.11.09	X1.0 2001.11.04 (16:03)	12.89	YYY	A1	$\beta\gamma$
09733	2001.12.08	2001.12.20	X6.2 2001.12.13 (14:20)	80.52	M	B3	$\beta\gamma\delta$
09906	2002.04.11	2002.04.21	X1.5 2002.04.21 (00:43)	19.72	YYY	A2	$\beta\gamma\delta$
09961	2002.05.19	2002.06.01	X2.1 2002.05.20 (15:21)	24.74	YYY	A2	$\beta\gamma\delta$
10017	2002.06.28	2002.07.05	X1.5 2002.07.03 (02:13)	39.75	M	B3	$\beta\gamma\delta$
10030	2002.07.09	2002.07.22	X3.0 2002.07.15 (20:08)	58.59	M	B2	$\beta\gamma\delta$
10039	2002.07.22	2002.08.04	X4.8 2002.07.23 (00:18)	54.15	M	B3	$\beta\gamma\delta$
10069	2002.08.11	2002.08.24	X3.1 2002.08.24 (00:49)	81.11	M	B3	$\beta\gamma\delta$
10095	2002.08.29	2002.09.10	X1.5 2002.08.30 (12:47)	17.11	YYY	A1	$\beta\gamma$
10314	2003.03.14	2003.03.21	X1.5 2003.03.17 (18:50)	64.62	M	B2	$\beta\gamma\delta$
10365	2003.05.20	2003.06.03	X3.6 2003.05.28 (00:17)	106.11	M	B3	$\beta\gamma\delta$
10375	2003.06.01	2003.06.14	X1.7 2003.06.09 (21:31)	100.44	M	B2	$\beta\gamma\delta$
10386	2003.06.15	2003.06 25	X1.3 2003.06.15 (23:25)	21.64	M	B3	$\beta\gamma\delta$
10484	2003.10.18	2003.10.31	X1.2 2003.10.26 (17:21)	51.33	M	B3	$\beta\gamma\delta$
10486	2003.10.22	2003.11.05	X17 2003.10.28 (09:51)	501.41	M	B3	$\beta\gamma\delta$
10488	2003.10.27	2003.11.04	X3.9 2003.11.03 (09:43)	98.00	M	B2	$\beta\gamma\delta$
10564	2004.02.21	2004.03.02	X1.1 2004.02.26 (02:03)	24.22	M	B2	$\beta\gamma\delta$
10649	2004.07.12	2004.07.25	X3.6 2004.07.16 (07:51)	102.07	δ	B2	$\beta\gamma\delta$
10656	2004.08.06	2004.08.19	X1.8 2004.08.18 (17:29)	91.48	M	B2	$\beta\gamma\delta$
10691	2004.10.24	2004.11.05	X1.2 2004.10.30 (11:38)	32.89	YYY	A2	$\beta\gamma\delta$
10696	2004.11.02	2004.11.12	X2.5 2004.11.10 (01:59)	101.00	M	B2	$\beta\gamma\delta$
10715	2004.12.28	2005.01.09	X1.7 2005.01.01 (00:01)	32.20	NYY	B1	$\beta\gamma\delta$
10720	2005.01.11	2005.01.21	X7.1 2005.01.20 (06:36)	215.27	δ	B2	$\beta\delta$
10786	2005.07.02	2005.07.14	X1.2 2005.07.14 (10:16)	44.22	M	B3	$\beta\gamma\delta$
10792	2005.07.29	2005.08.09	X1.3 2005.07.30 (06:17)	18.52	NNN	B1	$\beta\gamma\delta$
10808	2005.09.07	2005.09.19	X17 2005.09.07 (17:17)	353.63	M	B3	$\beta\gamma\delta$
10930	2006.12.06	2006.12.18	X9.0 2006.12.05 (10:18)	168.96	M	B3	$\beta\gamma\delta$

[a] For bipolar ARs, 'H' stands for the Hale polarity law, 'J' for the Joy law and 'L' for the leading spot prevalence rule. In this column, for bipolar ARs, 'Y' denotes 'Yes' (i.e. adhering to the law) and 'N' denotes 'No' (i.e. violation of the law). 'M' denotes multipolar ARs and 'δ' denotes ARs with tight a strong dominating δ-structure.
[b] The strongest flare occurred between two ARs.

a flare index above ≈100 level, so the data for irregular ARs only appear above this level.

To make this tendency more prominent, we calculated a yearly cumulative flare index as a sum of flare indices of all ARs of a given class (Fig. 8). Flare-producing ARs in the A class, which we hypothesize is a product of the global dynamo, tend to appear and contribute to the flaring at the rising phase and during the first maximum of a cycle, when the global toroidal field is expected to be strong. However, during the second maximum and the declining phase of a solar cycle, when the toroidal field weakens (Charbonneau 2020), the irregular ARs become the main producers of powerful episodes of solar activity.

Table 3. ARs with X-class flares in solar cycle 24.

NOAA	Start	End	Max. flare (UT)	FI	H J L[a]	MMC class	Hale class
11158	2011.02.11	2011.02.21	X2.2 2011.02.15 (01:44)	53.72	M	B2	$\beta\gamma\delta$
11166	2011.03.03	2011.03.16	X1.5 2011.03.09 (23:13)	24.74	M	B2	$\beta\gamma\delta$
11263	2011.07.28	2011.08.11	X6.9 2011.08.09 (07:48)	62.30	M	B2	$\beta\gamma\delta$
11283	2011.08.30	2011.09.12	X2.1 2011.09.06 (22:12)	43.55	YYY	A2	$\beta\gamma\delta$
11302	2011.09.22	2011.10.05	X1.9 2011.09.24 (09:21)	75.55	YYY	A2	$\beta\gamma\delta$
11339	2011.11.01	2011.11.15	X1.9 2011.11.03 (20:16)	37.92	YYY	A2	$\beta\gamma\delta$
11402	2012.01.14	2012.01.28	X1.7 2012.01.27 (17:37)	24.29	YYY	A1	$\beta\gamma$
11429	2012.03.03	2012.03.16	X5.4 2012.03.07 (00:02)	95.78	M	B2	$\beta\gamma\delta$
11515	2012.06.27	2012.07.09	X1.1 2012.07.06 (23:01)	89.70	YYY	A2	$\beta\gamma\delta$
11520	2012.07.07	2012.07.19	X1.4 2012.07.12 (15:37)	28.96	M	B3	$\beta\gamma\delta$
11598	2012.10.21	2012.11.02	X1.8 2012.10.23 (03:13)	28.74	YYY	A2	$\beta\delta$
11748	2013.05.13	2013.05.26	X3.2 2013.05.13 (23:59)	77.78	M	B3	$\beta\gamma\delta$
11875	2013.10.17	2013.10.30	X2.3 2013.10.29 (21:42)	61.85	YYY	A2	$\beta\gamma\delta$
11882	2013.10.25	2013.11.06	X2.1 2013.10.25 (14:51)	47.63	YNN	B1	$\beta\gamma\delta$
11890	2013.11.03	2013.11.16	X3.3 2013.11.05 (22:07)	61.41	YYY	A2	$\beta\gamma\delta$
11893	2013.11.09	2013.11.21	X1.0 2013.11.19 (10:14)	11.33	M	B3	$\beta\delta$
11944	2014.01.01	2014.01.14	X1.2 2014.01.07 (18:04)	32.15	M	B2	$\beta\gamma$
11990	2014.02.25	2014.03.10	X4.9 2014.02.25 (00:39)	39.26	δ	B2	$\beta\delta$
12017	2014.03.22	2014.04.03	X1.0 2014.03.29 (17:35)	14.81	YYY	A2	$\beta\delta$
12035	2014.04.11	2014.04.24	X1.3 2014.04.25 (00:27)	20.84	M	B3	$\beta\gamma$
12087	2014.06.10	2014.06.23	X2.2 2014.06.10 (11:36)	56.30	M	B3	$\beta\delta$
12158	2014.09.05	2014.09.18	X1.6 2014.09.10 (17:21)	17.18	NNY	B1	$\beta\gamma\delta$
12192	2014.10.18	2014.10.31	X3.1 2014.10.24 (21:07)	173.04	M	B3	$\beta\gamma\delta$
12205	2014.11.04	2014.11.17	X1.6 2014.11.07 (16:53)	54.52	M	B2	$\beta\gamma\delta$
12242	2014.12.14	2014.12.24	X1.8 2014.12.20 (00:11)	51.00	M	B3	$\beta\gamma\delta$
12297	2015.03.07	2015.03.20	X2.1 2015.03.11 (16:11)	81.26	M	B3	$\beta\gamma\delta$
12339	2015.05.05	2015.05.17	X2.7 2015.05.05 (22:11)	32.74	M	B2	$\beta\gamma$
12673	2017.08.30	2017.09.10	X9.3 2017-09-06 (11:53)	220.44	M	B3	$\beta\gamma\delta$

[a]For bipolar ARs, 'H' stands for the Hale polarity law, 'J' for the Joy law and 'L' for the leading spot prevalence rule. In this column, for bipolar ARs, 'Y' denotes 'Yes' (i.e. adhering to the law) and 'N' denotes 'No' (i.e. violation of the law). 'M' denotes multipolar ARs and 'δ' denotes ARs with tight a strong dominating δ-structure.

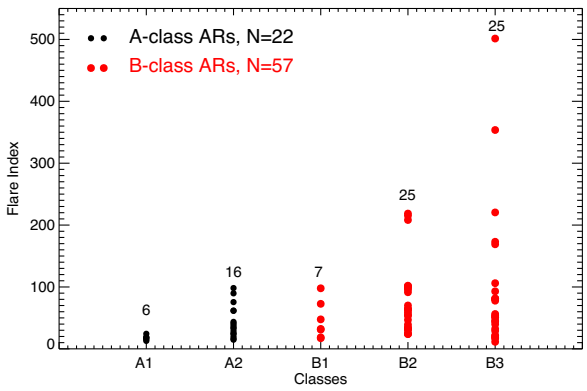

Figure 6. Distribution of 79 ARs with strong flares (>X1.0) over the MMC from class A1 to B3. Each AR is marked by a circle (black for regular ARs of A classes and red for irregular ARs of B classes). The vertical axis shows the flare index, FI, of each AR. For each class, numbers denote the number of cases. Strongest flares occur (FI > 100) only in ARs of classes B2 and B3.

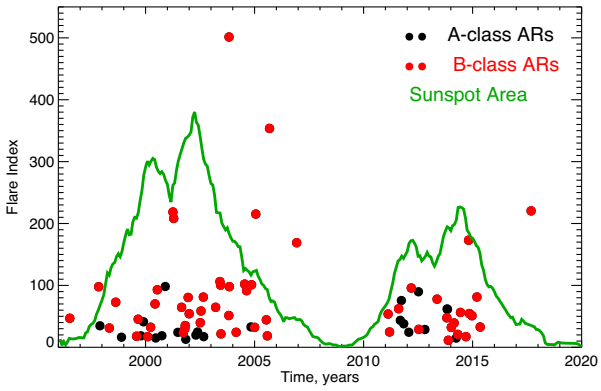

Figure 7. Time distribution of ARs with strong flares (>X1.0) along the two solar cycles. For each AR, the flare index FI is shown along the vertical axis. Regular (irregular) ARs are marked with black (red) circles. The green line shows the total sunspot area smoothed over 13 months; we used RGO and USAF/NOAA data, which are available at http://solarcyclescience.com/activeregions.html. Strongest flares (FI > 100) occur only during the second maximum and descending phase of a cycle.

5 CONCLUDING REMARKS

We have introduced an MMC of ARs in order to better describe the possible contribution of the turbulent dynamo to the formation of ARs. By comparing the MMC class of ARs and their flare productivity over solar cycles 23 and 24, we are able to conclude the following.

(i) Out of all ARs that produce X-class flares, 72 per cent are the AR 'violators', which are non-compliant with (at least one of) the empirical laws of the global dynamo (the Hale polarity law, the Joy law and the leading spot prevalence rule), while these ARs constitute only 25–30 per cent of all observed 1494 ARs (Abramenko et al. 2018). Thus, the strongest fluctuations in the time domain (flares) are statistically related to the strongest distortions in the

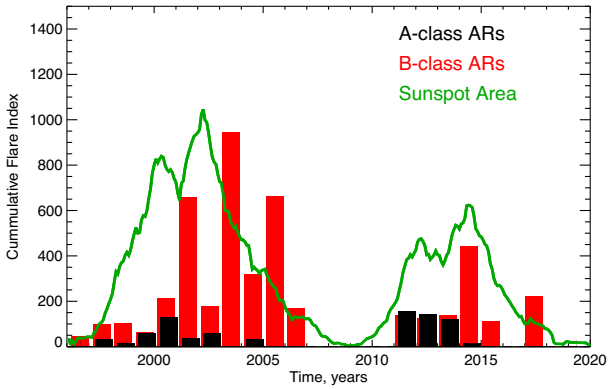

Figure 8. Flare index of regular (black) and irregular (red) ARs during the two solar cycles, cumulative over a year. Regular ARs (a product of the global dynamo) tend to contribute to strong flare production on the rising phase and during the first maximum of the cycle, whereas irregular ARs produce strong flares through the entire cycle and considerably enhance their activity during the second maximum and descending phase. Notations are the same as in Fig. 7.

space domain, which is one of the key properties of a non-linear dynamical dissipative system. The inference is in favour of the point of view that the solar dynamo is one of these systems.

(ii) The time distribution of flaring ARs over a solar cycle indicates that the regular ARs in the A class contribute to solar activity mostly during the rising phase of a cycle and its first maximum, whereas irregular ARs in the B class are more distributed in the decline phase and they are the dominating source of solar flares during the second maximum and the declining phase. The rising phase of the dynamo wave is when the toroidal component of the magnetic field is strongest so that we observe both regular and irregular flaring ARs. As the dynamo wave proceeds, the toroidal component weakens and the turbulent component of the dynamo becomes more pronounced, thus notably distorting the emerging toroidal flux tubes and leading to the appearance of strong fluctuations in the spatial domain (i.e. irregular ARs).

Our analysis has shown that the majority of ARs that produce X-class flares do not follow the laws of the global mean-field dynamo and possess an irregular magnetic structure. Therefore, large temporal and spatial fluctuations in the solar dynamo are not rare and indicate the existence of the turbulent component of the dynamo on scales of ARs. Thus, the gap between the large-scale dynamo that generates the global poloidal and toroidal fields and the small-scale turbulent dynamo that is responsible for quiet Sun magnetic fields may be filled by the turbulent dynamo acting on mid-scales throughout the convective zone. Then we might expect a continuous spectrum of turbulent magnetic fields and energy on a large range of spatial scales. The presumed continuous spectrum is a natural property of a turbulent medium (Monin & Yaglom 1975). Note that existence of a continuous temporal spectrum of solar activity was recently demonstrated by Frick et al. (2020) based on time variations of the total sunspot area. The continuous spectrum implies that magnetic energy is generated not only on the largest scales, but also on a wide range of intermediate scales of the turbulent intermittent convective zone. The entire process works as a whole with a continuous energy exchange between the scales. The concept was suggested in early theoretical studies by Kazantsev (1968) and Zel'dovich & Ruzmajkin (1987). More recently, the existence of the turbulent component of dynamo follows from theoretical considerations and numerical simulations in both time variations (Sokoloff et al. 2010; Olemskoy & Kitchatinov 2013; Passos et al. 2014; Karak & Miesch 2017; Schüssler & Cameron 2018) and spatial properties (Nelson et al. 2013) of solar activity. However, observational evidence of the continuous spectrum, especially in the spatial domain, is not strong so far, mainly because the dynamo action is hidden below the photosphere. Publications in this field are scarce (Sokoloff, Khlystova & Abramenko 2015).

In conclusion, it is worth mentioning that the four essential properties explored here, which characterize the regular ARs (bipolarity and three empirical laws), do not cover the entire list of such properties. For example, the hemispheric sign preference rule of helicity complies for the majority of ARs (see Pevtsov et al. 2014, and references therein). This parameter undoubtedly deserves an extended analysis in future. Note that LaBonte, Georgoulis & Rust (2007) have investigated the ARs of solar cycle 23 and found that for X-flaring ARs, the hemispheric sign preference rule tends to be obscured due to intrinsic helicity injection of opposite sign. A recent study by Park, Leka & Kusano (2021) of the hemispheric sign preference rule for ARs of solar cycle 24 demonstrated that in heliographic areas where the ARs with strong flares occurred, the degree of compliance of this rule is lowered. They argued that below the photosphere there should be localized volumes of enhanced turbulence, where vigorous turbulent plasma motions affect the shape and future flare capability of some flux tubes while they are rising to the surface. This inference is in agreement with the concept suggested above about the role of the turbulent component of the dynamo in AR formation and flaring.

ACKNOWLEDGEMENTS

I am grateful to an anonymous referee whose comments helped much to improve the paper. The *SDO* is a mission for the NASA Living With a Star (LWS) programme. The *SDO*/HMI data were provided by the Joint Science Operation Center (JSOC). The study was supported by the Russian Science Foundation grant 18-12-00131.

DATA AVAILABILITY

The MDI and HMI data that support the findings of this study are available in the Joint Science Operations Center (http://jsoc.stanford.edu/) and can be accessed under the 'open for all' data policy. Derived data products supporting the findings of this study are available from the author on request.

REFERENCES

Abramenko V. I., 2005, ApJ, 629, 1141
Abramenko V. I., Zhukova A. V., Kutsenko A. S., 2018, Geomagnetism and Aeronomy, 58, 1159
Babcock H. W., 1961, ApJ, 133, 572
Barnes G. et al., 2016, ApJ, 829, 89
Brun A. S., Browning M. K., Dikpati M., Hotta H., Strugarek A., 2015, Space Sci. Rev., 196, 101
Cameron R. H., Duvall T. L., Schüssler M., Schunker H., 2018, A&A, 609, A56
Charbonneau P., 2010, Living Reviews in Solar Physics, 7, 3
Charbonneau P., 2014, ARA&A, 52, 251
Charbonneau P., 2020, Living Reviews in Solar Physics, 17, 4
Cinto T., Gradvohl A. L. S., Coelho G. P., da Silva A. E. A., 2020, Solar Phys., 295, 93
D'Silva S., Choudhuri A. R., 1993, A&A, 272, 621
Falconer D. A., Moore R. L., Gary G. A., 2008, ApJ, 689, 1433

Frick P., Sokoloff D., Stepanov R., Pipin V., Usoskin I., 2020, MNRAS, 491, 5572
Frisch U., 1995, Turbulence: The Legacy of A. N. Kolmogorov. Cambridge University Press, Cambridge
Georgoulis M. K., 2012, Solar Phys., 276, 161
Hale G. E., Nicholson S. B., 1925, ApJ, 62, 270
Hale G. E., Ellerman F., Nicholson S. B., Joy A. H., 1919, ApJ, 49, 153
Ireland J., Young C. A., McAteer R. T. J., Whelan C., Hewett R. J., Gallagher P. T., 2008, Solar Phys., 252, 121
Ishii T. T., Kurokawa H., Takeuchi T. T., 1998, ApJ, 499, 898
Karak B. B., Miesch M., 2017, ApJ, 847, 69
Kazantsev A. P., 1968, Sov. Phys. JETP, 26, 1031
LaBonte B. J., Georgoulis M. K., Rust D. M., 2007, ApJ, 671, 955
Leighton R. B., 1969, ApJ, 156, 1
Leka K. D. et al., 2019, ApJ, 881, 101
McAteer R. T. J., Gallagher P. T., Conlon P. A., 2010, Adv. Space Res., 45, 1067
McClintock B. H., Norton A. A., 2013, Solar Phys., 287, 215
McIntosh P. S., 1990, Solar Phys., 125, 251
Monin A. S., Yaglom A. M., 1975, in Lumley J., ed., Statistical Fluid Mechanics: Mechanics of Turbulence. MIT Press, Cambridge, MA
Nelson N. J., Brown B. P., Brun A. S., Miesch M. S., Toomre J., 2013, ApJ, 762, 73
Nishizuka N., Kubo Y., Sugiura K., Den M., Ishii M., 2020, ApJ, 899, 150
Olemskoy S. V., Kitchatinov L. L., 2013, ApJ, 777, 71
Park S-H., Leka K. D., Kusano K., 2021, ApJ, 911, 79
Passos D., Nandy D., Hazra S., Lopes I., 2014, A&A, 563, A18
Pevtsov A. A., Berger M. A., Nindos A., Norton A. A., van Driel-Gesztelyi L., 2014, Space Sci. Rev., 186, 285
Pipin V. V., 2018, J. Atmos. Solar-Terrestrial Phys., 179, 185
Scherrer P. H. et al., 1995, Solar Phys., 162, 129
Schou J. et al., 2012, Solar Phys., 275, 229
Schüssler M., Cameron R. H., 2018, A&A, 618, A89
Sokoloff D., Arlt R., Moss D., Saar S. H., Usoskin I., 2010, in Proc. IAU Symp. Vol. 264, Solar and Stellar Variability: Impact on Earth and Planets. Kluwer, Dordrecht, p. 111
Sokoloff D., Khlystova A., Abramenko V., 2015, MNRAS, 451, 1522
Toriumi S., Wang H., 2019, Living Reviews in Solar Physics, 16, 3
Toriumi S., Schrijver C. J., Harra L. K., Hudson H., Nagashima K., 2017, ApJ, 834, 56
van Driel-Gesztelyi L., Green L. M., 2015, Living Reviews in Solar Physics, 12, 1
Wang Y-M., Sheeley N. R., 1991, ApJ, 375, 761
Zel'dovich Y. B., Ruzmajkin A. A., 1987, Usp. Fiz. Nauk, 152, 263
Zhukova A., Khlystova A., Abramenko V., Sokoloff D., 2020, Solar Phys., 295, 165
Zirin H., Liggett M. A., 1987, Solar Phys., 113, 267

This paper has been typeset from a TEX/LATEX file prepared by the author.